Infrared Emission Detection for Unknown Pulsar

João Carlos Schymura Gomes de Almeida,[1]★
[1]School of Physics and Astronomy, University of Southampton, University Road, Southampton SO17 1BJ, UK

Accepted XXX. Received YYY; in original form ZZZ

ABSTRACT

A fast Fourier transform (FFT) was performed to detect the infrared emission of an unknown pulsar. The largest peak on the FFT, at ≈ 60Hz, establishes the detection of the pulsar with a significance of 5.65σ. Two interpretations for the rotational frequency of the pulsar are presented and persued. Using the analysis of variance for period search method (AoV) around 60Hz, a frequency of 59.59 ± 0.98Hz was found. The frequency coincides within a standard deviation to the rotational frequency of PSR J1748-2021B in NGC 6440 globular cluster. An alternative interpretation arises from the light curve analysis, which indicates the existence of a subpulse. The existence of a pulse and subpulse at 29.88 ± 0.98Hz would make it the frequency of the fundamental harmonic and make the peak at 59.59 ± 0.98Hz correspond to the first harmonic. Recommendations for further observations are provided to confirm either interpretation and enhance understanding of this pulsar's unique characteristics.

Key words: Fourier Transform – Pulsar – Analysis of Variance

1 INTRODUCTION

Infrared (IR) emission flux data for an unknown pulsar was analysed. 256 datapoints were made available with a sampling rate of 4ms, totalling 1024 milliseconds of data. By performing a fast Fourier transform (FFT), the detection of the pulsar was confirmed to a 5.65 σ significance level. Its period of rotation and lightcurve were analysed via the analysis of variance for period search method (AoV) (Schwarzenberg-Czerny 1989). Pulsars, rapidly rotating neutron stars with strong magnetic fields, emit beams of radiation that are observed as periodic pulses. The precise periodicity of a pulsar's signals makes their rotational frequency detectable.

1.1 Fast Fourier Transform

The fast Fourier transform (FFT) algorithm, popularised by Cooley & Tukey (1965) [1], makes use of several symmetries in the coefficients of the Fourier transform to increase performance. As a result, it manages to reduce the complexity of computing the direct fourier transform (DFT) from $O(n^2)$, which arises if one simply applies the definition of DFT to $O(n \log n)$, where n is the number of data points. Brault & White (1971) introduced the fast Fourier transform (FFT) to astronomy.

1.2 Analysis of Variance (AoV)

Given Fourier transforms are more suited to detect sinusoidal signals, and pulsar pulse profiles are not in general sinusoidal (Lyne & Manchester 1988), an AoV was used. Executing the AoV requires folding and binning data with a range of trial periods. The optimum period is chosen as the one that maximises the χ^2 compared to a constant signal. This method assumes that by choosing a non optimum frequency, the errors will cancel out. However, around the optimum frequency that is not the case, as constructive interference would lead to a non constant pulse peak profile.

1.3 Pulsars

Pulsars were first detected by PhD student Jocellyn Brunell (HEVVISH et al. 1968). As of May 2024, more than 3500 pulsars have been found and their periods catalogued (ATNF 2024; Manchester et al. 2005). Pulsars' characteristic fast rotation is inherited from the angular-momentum conservation from their progenitor star. Given that their radius shrinks to ≈ 11km (Bose et al. 2018), and that moment of inertia, I, follows $I \propto R^2$, their angular velocity grows according to $\omega \propto 1/R^2$. Pulsar frequencies have been known to reach as high as 716 Hz (Hessels et al. 2006).

Pulsars are neutron stars with a strong magnetic field, varying from 10^{11} to 10^{13} Gauss (White et al. 2022). Magnetic fields are believed to accelerate electrons that leave through their poles. This acceleration leads to synchotron radiation as seen on Figure 1. This emission can be inverse Compton scattered up to gamma ray energies by high energy particles leaving the pulsar poles, making the beams visible all across the electromagnetic spectrum (Lyutikov 2013).

Given the pulsars rotational axis and magnetic poles are misaligned, observers can detect this radiation periodically. Caution is necessary when measuring the period between pulsar beam detec-

★ E-mail: jsga1n21@southampton.ac.uk

[1] Interestingly, Gauss discovered the FFT in 1805 (Heideman et al. 1984; Gauss 1866), before Fourier "discovered" the Fourier transform in his famous Théorie analytique de la chaleur, originally published in 1822 (Fourier 1888).

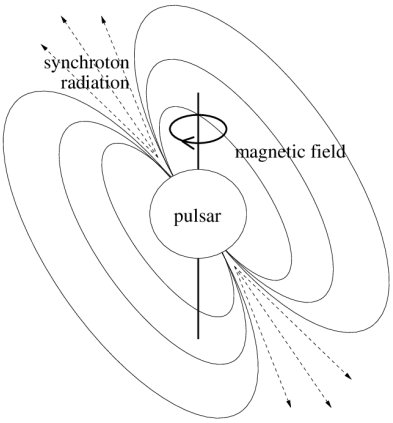

Figure 1. Basic schematic of a pulsar. It shows its main features including its magnetic field lines and the direction of the synchotron radiation jets. Note the misalignment between the magnetic pole and the rotational axis. Taken from Ruester (2006), based on Rüster (2003).

tions, as subpulses, subharmonics and higher harmonics may be observed. Subpulses are an area of active research with various models with varying emission mechanisms (Ruderman & Sutherland 1975; Arons & Scharlemann 1979; Gil et al. 2003).

2 METHODS

To test for methodological validity, synthetic code was used before analysing the observational data. Chosen synthetic data consisted mainly of a sinusoidal function, with known frequency of 100Hz, with additional randomly generated noise. A FFT was performed on the data (Cooley & Tukey 1965; Press 2007), resulting in the power spectrum seen in Figure 2.

The probability of a peak being statistically significant, as opposed to a statistical fluke, was tested by measuring the proportion of randomly arranged values being above the power of the top 3 peaks. The statistical significance of each peak was tested using 100 million simulations of the data points. This involved randomly shuffling the time coordinates of each data point while maintaining their amplitude coordinates during each simulation (Harris et al. 2020). These tests were first performed on synthetic data to certify the validity of our code. After confirmation, the IR's data peaks were analysed. The maximum values of each power spectrum were recorded and their counts can be seen in Figure 4.

2.1 Main Assumptions

It was assumed that the frequency resolution was the main factor of error, and that statistical errors were not significant. In the FFT power spectrum (Figure 3), it was assumed that the neighbouring bins, 59.6Hz and 60.5Hz corresponded to the same signal and the signals of all other frequencies were considered independent. Parseval's theorem states that the total energy of the whole signal is conserved (Parseval 1806), meaning each frequency is not actually independent, making this an approximation. For light curves, noise was assumed to be random and described by a Gaussian distribution with time invariant parameters. No binary companions with time varying emission was considered.

2.2 Analysis of Variance (AoV)

The AoV was performed based on Schwarzenberg-Czerny (1989)'s original method. It consisted of folding the data based on a certain frequency, and binning the resultant light curve in bins of equal width - in this case 15 bins. The optimum frequency was found by finding the maximum χ^2 between the folded curve and a its mean amplitude. The χ^2 test was performed using test frequencies within the range of the FFT's highest frequency peaks (from 58Hz to 62Hz). Another region of frequency space was analysed, from 28Hz to 32Hz, corresponding to another candidate for the fundamental frequency.

3 RESULTS

After the code was validated for synthetic data, the same method was applied to the actual data, with the FFT power spectrum seen in Figure 3. The significance of the three main peaks at 59.6, 60.5, 30.3Hz were evaluated to be 4.69, 2.76, 1.30 σ respectively. Given the 60.5 and 59.6 Hz bins are adjacent, their signal significance level was combined to be 5.65 σ, computed as independent results. How these peak powers compare to random simulations is displayed in Figure 4.

A light curve was then plotted with the optimum frequency. The optimum frequency, that maximised χ^2, was 59.59Hz, corresponding

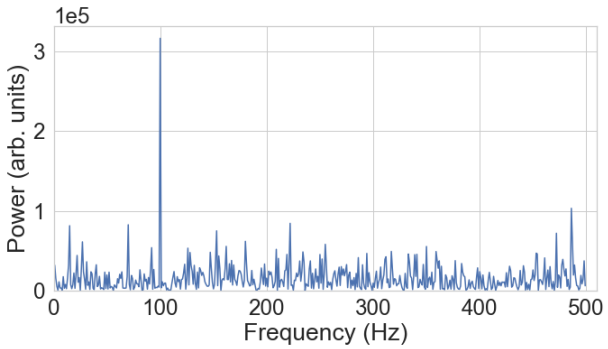

Figure 2. Power spectrum of artificial data showing the peak at 100Hz, which coincides with the introduced signal. All positive frequencies are reproduced.

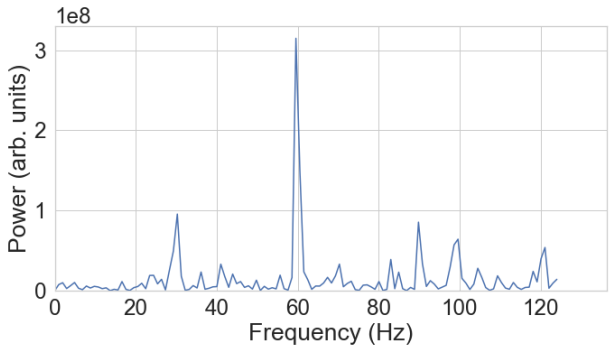

Figure 3. Power spectrum of IR data after a FFT. Note the highest peak at ≈ 60Hz and some minor peaks at ≈ 30, 90, 100 and 120Hz.

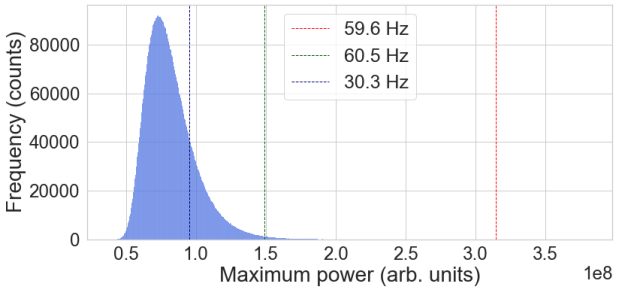

Figure 4. Histogram showing the number of simulations that had a specific maximum power. Vertical lines correspond to the values for the three maximum frequencies of the power spectrum of the original data

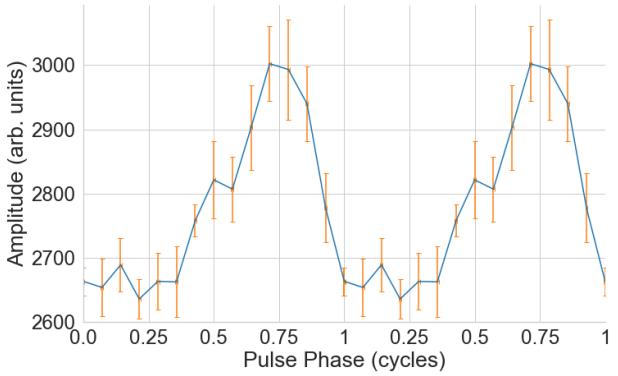

Figure 5. Light curve, folded with frequency = 59.59Hz (period = 16.78ms). 15 bins were used and the errors (in orange) represent the standard error of the mean. Two phase cycles are shown for clarity.

to a period of 16.73 ms. Folded data was binned in 15 equal bins and its light curve can be seen in Figure 5. The same process was done for frequencies ≈ 30Hz, resulting in a frequency maximising χ^2 of 29.88Hz (light curve shown in Figure 6).

3.1 Errors on Frequency Estimate

Frequency resolution was assumed to be the dominant source of error in data after the FFT was performed. Given the peak was of 5.65 σ significance, it is also safe to assume that noise had little impact in finding the estimate of frequency. Frequency resolution is defined as:

$$\Delta f = \frac{f_s}{N} = \frac{250}{256} = 0.977Hz \quad (1)$$

Where f_s is the sampling rate in samples per second and N is the number of samples taken. Statistical errors are displayed after binning, and included in Figures 5 and 6.

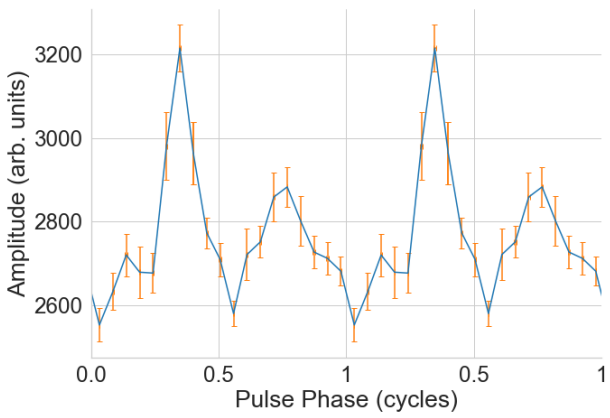

Figure 6. Light curve, folded with frequency = 29.88Hz (period = 33.47ms), approximately half of the fundamental frequency (double the period) seen in Figure 5. Evidence for a subpulse at phase ≈ 0.7. 20 bins were used and the errors represent the standard error of the mean. Two phase cycles are shown for clarity.

4 DISCUSSION

The combined 5.65 σ detection validates the existence of the pulsar. Light curve analysis may lead to two interpretations of the data. One interpretation is that the pulse has a frequency of 59.59 ± 0.98Hz with a light curve as shown in Figure 5. The other interpretation on the data can be that the rotational frequency of the pulsar is 29.88 ± 0.98Hz, with a light curve as shown in Figure 6. In the later scenario, the peak seen at 59.59 ± 0.98Hz would correspond to the first excited harmonic.

4.1 Is the Pulsar PSR J1748-2021B?

The first interpretation, with a estimated rotational frequency of 59.59 ± 0.98Hz is motivated by the strength of the frequency signal of the peak found after the FFT. The peak at ≈60Hz had a statistical significance of 5.65 σ, with the peak of the alternative 30.3Hz at only 1.30 σ. This discrepancy makes the peak at ≈60Hz the only statistically significant peak. In this case, the peak at 30.3Hz is a candidate for a subharmonic, who's existence is common within pulsars (Strohmayer & Markwardt 2002).

If considering the fundamental frequency at 59.59 ± 0.98Hz, its period (16.78 ± 0.28ms) lies within one standard deviation of the estimate of the period found by Freire et al. (2008) for the PSR J1748-2021B pulsar at 16.76 ms, which relied on radio observations. This pulsar has significant properties to justify such attention. It is potentially the heaviest known pulsar, with initial estimate at $2.74^{+0.21}_{-0.21} M_\odot$ Freire et al. (2008), but since revised to $2.548^{+0.047}_{-0.078} M_\odot$ (Clifford 2019). Its significance is such that it has been proposed to be observed in the JWST by the authors credited with its discovery (Freire et al. 2021).

4.2 Possibility for Subpulses

The behaviour of pulsar subpulses is an active area of research (Tian et al. 2024). It is believed they are related to the emission mechanisms in the pulsar (Weltevrede et al. 2006). Figure 6 may be interpreted as the existence of a subpulse, approximately 1/3 of the height of the

main pulse. More data would be necessary to confirm the existence of the subpulse and observe its properties, such as possible subpulse drifting – observed in approximately 40 to 50% of pulsars (Basu et al. 2019).

This interpretation of the data would lead to a frequency of approximately half that of the one assumed on Section 4.1 as only the main pulse is considered when finding the frequency. This interpretation could suggest an explanation for the higher power observed at ≈ 60Hz – this being the constructive interference of the subpulse and pulse. This can be seen in Figure 6 with the pulse and subpulse being approximately half a period apart. There are multiple known pulsars within 1 σ of the frequency estimate 29.88 ± 0.98Hz (ATNF 2024), so pinpointing a specific pulsar is not possible if this interpretation holds true.

5 CONCLUSIONS

As has been demonstrated with the available IR data, a pulsar was detected with the confidence level of 5.56 σ for it's peak ≈ 60Hz. Two interpretations were posed in section 4 for the period/frequency of said pulsar. One of them being that its rotational frequency is 59.59 ± 0.98Hz, and the 1.3 σ peak observed at ≈ 30Hz corresponds to a subharmonic, a behaviour that appears on FFT of pulsar data (Strohmayer & Markwardt 2002). The only known pulsar to display this value for rotational frequency is PSR J1748-2021B.

However, figure 6 points at the existence of a pulse and a subpulse, which if confirmed would indicate a fundamental frequency of 29.88 ± 0.98Hz. The alternative explanation would treat the 59.59 ± 0.98Hz peak as a higher harmonic. Further observations are necessary to confirm the correct interpretation of the current data, with more observational time, as only 1 second of data was available, or different parts of the electromagnetic spectrum.

DATA AVAILABILITY

Data supporting this study is openly available from a repository in Github (Schymura Gomes de Almeida 2024).

REFERENCES

ATNF A. T. N. F., 2024, ATNF Pulsar catalogue, https://www.atnf.csiro.au/research/pulsar/psrcat/

Ahmadianfar I., et al., 2023, Sustainability, 15, 1825

Aristoff J. M., Horwood J. T., Poore A. B., 2015, Celestial Mechanics and Dynamical Astronomy, 122, 169

Arons J., Scharlemann E. T., 1979, Astrophysical Journal, Part 1, vol. 231, Aug. 1, 1979, p. 854-879., 231, 854

Basu R., Mitra D., Melikidze G. I., Skrzypczak A., 2019, Monthly Notices of the Royal Astronomical Society, 482, 3757

Blanes S., Casas F., Farres A., Laskar J., Makazaga J., Murua A., 2013, Applied Numerical Mathematics, 68, 58

Bose S., Chakravarti K., Rezzolla L., Sathyaprakash B., Takami K., 2018, Physical review letters, 120, 031102

Brault J., White O., 1971, Astronomy and Astrophysics, Vol. 13, p. 169 (1971), 13, 169

Brummer A. B., Hunt D., Savage V., 2020, IEEE Transactions on Medical Imaging, 40, 297

Clifford N., 2019, PhD thesis

Cooley J. W., Tukey J. W., 1965, Mathematics of computation, 19, 297

Ding Y., Zhu L., Zhang X., Ding H., 2011

Dormand J. R., Prince P. J., 1980, Journal of computational and applied mathematics, 6, 19

Fourier J. B. J., 1888, Théorie analytique de la chaleur. Vol. 1, Gauthier-Villars

Freire P. C., Ransom S. M., Bégin S., Stairs I. H., Hessels J. W., Frey L. H., Camilo F., 2008, The Astrophysical Journal, 675, 670

Freire P. C. C., et al., 2021, Confirming the most massive neutron star with observations of its companion, JWST Proposal. Cycle 1, ID. #2204

Gauss C. F., 1866, Carl Friedrich Gauss Werke, 3, 265

Giampaoli I., Ng W. L., Constantinou N., 2009, Finance Research Letters, 6, 47

Gil J., Melikidze G. I., Geppert U., 2003, Astronomy & Astrophysics, 407, 315

HEVVISH A., PILKINGTON J., COLLINS R., 1968, NATURE, 217

Harris C. R., et al., 2020, Nature, 585, 357

Heideman M., Johnson D., Burrus C., 1984, IEEE Assp Magazine, 1, 14

Hessels J. W., Ransom S. M., Stairs I. H., Freire P. C., Kaspi V. M., Camilo F., 2006, Science, 311, 1901

Lee M.-C., Su J.-B., Liu H.-C., 2008, Applied Financial Economics Letters, 4, 425

Levin D., 1996, Journal of Computational and Applied Mathematics, 67, 95

Lyne A., Manchester R., 1988, Monthly Notices of the Royal Astronomical Society, 234, 477

Lyutikov M., 2013, Monthly Notices of the Royal Astronomical Society, 431, 2580

Madejová J., 2003, Vibrational spectroscopy, 31, 1

Manchester R. N., Hobbs G. B., Teoh A., Hobbs M., 2005, The Astronomical Journal, 129, 1993

Milotti E., Del Fabbro A., Chignola R., 2009, Computer Physics Communications, 180, 2166

Movasaghi Z., Rehman S., ur Rehman D. I., 2008, Applied Spectroscopy Reviews, 43, 134

Munthe-Kaas H., 1999, Applied Numerical Mathematics, 29, 115

Parseval M.-A., 1806, Mém. prés. par divers savants, Acad. des Sciences, Paris,(1), 1, 42

Prajna K., Mukhopadhyay C., 2020, Journal of Nondestructive Evaluation, 39, 14

Press W. H., 2007, Numerical recipes 3rd edition: The art of scientific computing. Cambridge university press

Qiao Z., Li L., Zhao X., Liu L., Zhang Q., Shili H., Atri M., Li X., 2023, Computers in Biology and Medicine, 160, 106949

Rangkuti Y. M., Huda A., 2020, in Journal of Physics: Conference Series. p. 012025

Ruderman M., Sutherland P. G., 1975, Astrophysical Journal, vol. 196, Feb. 15, 1975, pt. 1, p. 51-72., 196, 51

Ruester S. B., 2006, arXiv preprint nucl-th/0612090

Rüster S. B., 2003, PhD thesis, Frankfurt am Main, Johann Wolfgang Goethe-Univ., Diplomarbeit, 2003

Schwabacher A. W., Shen Y., Johnson C. W., 1999, Journal of the American Chemical Society, 121, 8669

Schwarzenberg-Czerny A., 1989, Monthly Notices of the Royal Astronomical Society, 241, 153

Schymura Gomes de Almeida J. C., 2024, Infrared emission detection for pulsar, https://github.com/Joao-Carlos-S-G-de-A/Pulsar-Fourier-Transform/

Simos T., Aguiar J. V., 2001, Journal of mathematical chemistry, 30, 121

Strohmayer T. E., Markwardt C. B., 2002, The Astrophysical Journal, 577, 337

Tian P.-F., Zhang P., Yang W., Wang W., Wang P., 2024, Journal of High Energy Astrophysics, 42, 27

Weltevrede P., Edwards R., Stappers B., 2006, Astronomy & Astrophysics, 445, 243

White C. J., Burrows A., Coleman M. S., Vartanyan D., 2022, The Astrophysical Journal, 926, 111

Zhang Y. Y., Zhang L., Shang Z. Q., Su Y. R., Wu Z., Yan F. B., 2022, Publications of the Astronomical Society of the Pacific, 134, 034502

APPENDIX A: ADDENDUM

A1 Use in Academia

A1.1 Integration

Levin (1996) proposes a new approach to evaluate oscillatory integrals. This class of integrals involve rapidly oscillating functions. Examples that include oscillatory integrals include phenomena like interference patterns, which are applied in many areas of physics. The new method takes inspiration from quantum mechanics, condensed matter physics, and quantum gravity methods, performing path integrals with a similar fashion.

In order to simulate large-scale biophysical simulations, several time integrals of ODEs are necessary. Milotti et al. (2009) simulates the growth of three-dimensional tumor cell aggregates (spheroids). The challenge comes from cellular events that have timescales that span $\approx$ 12 orders of magnitude. To do that, numerical integrations must be applied routinely.

Blanes et al. (2013) introduces new methods for numerical integration particularly for N-body problems. These are part of a class of methods called splitting methods, intended for differential equations that can be subdivided into smaller, easier to solve numerical problems. These methods greatly increase efficiency, as solving multiple differential equations is computationally intense, such as in n-body simulations.

A1.2 Runge-Kutta

In mathematics, Runge-Kutta (R-K) methods are used to study manifolds. Manifolds are collections of points that form sets such as closed surfaces. Munthe-Kaas (1999) proves that any classical Runge-Kutta method can be transformed into a method of the same order on a general homogeneous manifold and present use cases and applications.

Aristoff et al. (2015) devised a method for uncertainty propagation using the R-K method. It was initially tested for to a perturbed two-body problem in orbital mechanics. Results show that given it does not solve each initial value problem (a differential equation) individually, instead doing it collectively, this method significantly reduces the computational cost of propagating errors.

In the interface of physics and chemistry, Simos & Aguiar (2001) used R-K methods to numerically solve the Schrödinger equation. Based on previous work by Dormand & Prince (1980), Simos & Aguiar modified the algorithm, becoming more efficient in solving the Schrödinger equation.

A1.3 Fourier Transforms

Radio astronomy have commonly used FFTs since it was popularised by Brault & White (1971). 50 years have passed, yet adapting it to each problem is still a active area of research. Zhang et al. (2022) wrote a new algorithm to perform real-time FFT for solar radio observations. They found a overal reduction in resource usage, including a 37% reduction in RAM usage compared to general FFT algorithms when applied to solar radio observations.

Fourier transform infrared (FTIR) spectroscopy is employed in various areas of science. In biology, biological tissue is studied by measuring the scattering of photons on tissue (Movasaghi et al. 2008). Characteristic peaks observed are catalogued on Movasaghi et al.'s paper and can be used as reference to aid other researchers in the field.

In chemistry, Schwabacher et al. (1999) used to create libraries of useful compounds. Schwabacher et al. identified the problem of having an enormous amount of data and having to test and analyse so much data. In a creative solution they positioned reagents in different repeating patterns as threads wrapped around two cylinders as seen in figure A1, forming all reactions. Given the patterns were repetitive, they could perform FFT to the data and get the molecules with the most desired properties. This can assist the development of new drugs, materials and catalysts.

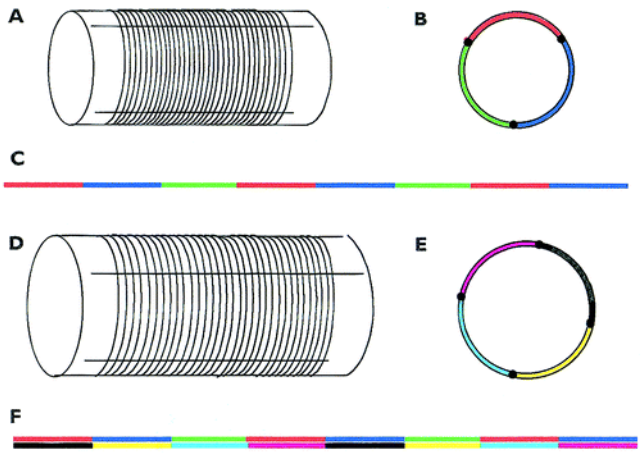

Figure A1. Cylinders with varying threads and repetition patterns. Below shows how superimposing both threads makes all combinations possible. Taken from Schwabacher et al. (1999).

A2 Use in Industry

A2.1 Integration

In hope of diagnosing vascular diseases, Brummer et al. (2020) measure the tortuosity of blood vessels, the curved and twisted shape of the vessel. They do that by performing numerical integrations of the Frenet-Serret equations. Where the Frenet-Serret equations are a set of differential equations used to describe the curvature and torsion of a curve in three-dimensional space.

Lee et al. (2008) estimates a quantity called Value at Risk (VAR) in US stocks. Where VAR is the maximum potential maximum potential loss that could incur within a certain confidence level. In that paper they set 95, 99 and 99.5% as the confidence levels that you would not loose more than set amounts. To perform this estimate they had to integrate the area under a curve until it got to the desired confidence level. For that they performed numerical integration utilising a adapted Simpson's rule algorithm.

Ding et al. (2011) applied numerical integration techniques to milling. When a milling tool cuts away material, its stability may be compromised as vibrations dominate a so called *forced vibration phase*. They estimate the milling dynamics in the form of an integral equation. Then a gauss numerical integral was performed to estimate this integral equation to then predict the *milling stability*.

A2.2 Runge-Kutta

Rangkuti & Huda (2020) used R-K to analyse a *hyperchaotic finance system*(HFS). The HFS is represented by a dynamic model involving interest rates, investment demand, and price index, is analyzed using differential equations. These are solved by the R-K methods

that are then compared, with the fifth order improved R-K (IRK5) outperforming previous R-K techniques.

Ahmadianfar et al. (2023) used used R-K to solve water engineering optimisation. In the article they propose a optimisation algorithm they name enhanced multioperator Runge–Kutta optimization (EMRUN). EMRUN builds upon classical RK methods but add adaptive parameters and a range of new techniques. EMRUN, tailor fit to water optimisation problems, arrives to 99.99% of the global solution faster and more precisely than comparable non-RK methods.

With the aim to perform accurate medical diagnosis, Qiao et al. (2023) used R-K techniques within a machine learning algorithm. Qiao et al. identified setting hyperparameters to the machine learning model as great source of error. To improve it, a R-K optimiser was used to adaptively adjust the hyperparameters of the machine learning methods, yielding more accurate diagnoses.

A2.3 Fourier Transforms

Applied to the field of material science, Madejová (2003) used Fourier-transform infrared spectroscopy (FTIR) to distinguish the proprieties of clay minerals. FTIRs produces a spectrum found by applying a Fourier transform to the absorption or emission spectra. Using these spectra they could derive information concerning their structure, composition, and the structural changes that occur after some chemical modifications.

In the subject of acoustics, Prajna & Mukhopadhyay (2020) studied methods to improve the acoustic emission technique (AET). AET is a method of detecting crack growth and monitoring the structural integrity of various components. This method is affected by background noise that reduce the signal to noise ratio, thus making detections harder. To treat noise, the signal has to pass through a Fourier transform, to pass through various noise reduction methods compared in this paper.

Giampaoli et al. (2009) applies Fourier analysis techniques to analyse ultra-high-frequency (UHF) financial data. Traditional methods struggle with high frequency data, leading to substantial information loss, as after resampling or interpolation. They compare Fourier transform algorithms, revealing that using the Lomb–Scargle Fourier transform on irregularly spaced UHF data provides more accurate spectral density estimates. These were compared to traditional Fourier analysis methods applied after resampling or interpolation, necessary to apply certain Fourier transform algorithms.

This paper has been typeset from a TEX/LATEX file prepared by the author.